Supporting Information

Visualization of bubble-induced mass transport at vertical hydrogen evolving electrodes

Jorrit Bleeker[1], Florianne M. Wiegel[1], Aron P. Kahn[1], J.W. Haverkort[2], Christiaan V. Schinkel[1], Maxime Hoogland[1], Lorenz M. Baumgartner[1], Wolter F. Jager[1], J. Ruud van Ommen[1], David A. Vermaas [1,*]

[1]Department of Chemical Engineering, Delft University of Technology, 2629 HZ Delft, The Netherlands

[2]Department of Process and Energy, Delft University of Technology, 2628 CB Delft, The Netherlands

*Corresponding Author, email: D.A.Vermaas@tudelft.nl

Table of contents:

SI-1. Photos of the setup

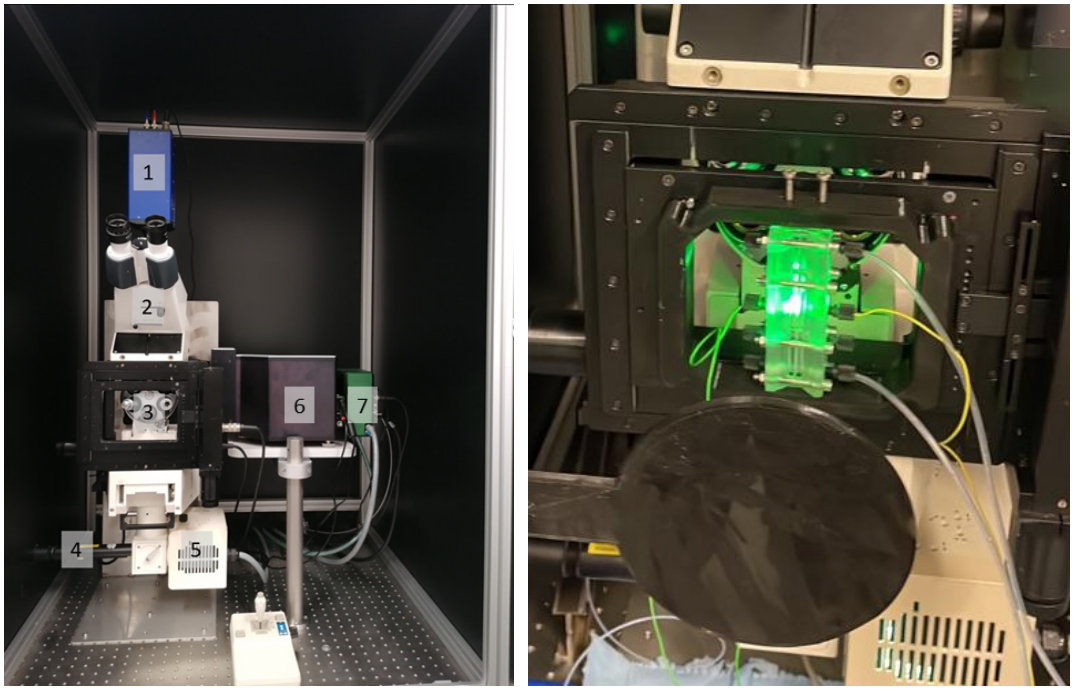

Figure S1. (Left) Photograph of the setup with **1.** µPIV camera **2.** Microscope **3.** 3D printed holder for the electrolyser on a movable plate (controlled with joystick) and lens objectives. This holder can be replaced with a 3D holder for a cuvette **4.** µPIV Laser **5.** Halogen lamp (used when setting up and focussing) **6.** Spinning disk confocal unit **7.** FLIM camera **(Right)** Photograph of the setup during µPIV operation

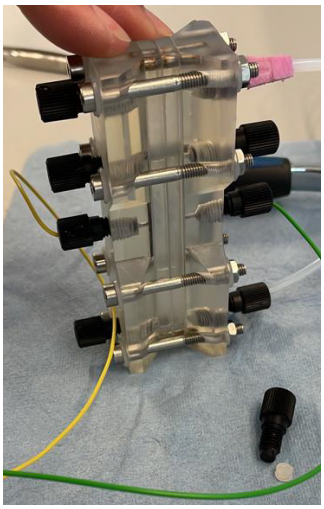

Figure S2. Photograph of the empty transparent flow cell for µPIV.

SI-2. µPIV method explanation

In this section we explain the µPIV method, from taking the images up to obtaining the velocity profile, see **Figure S3**:

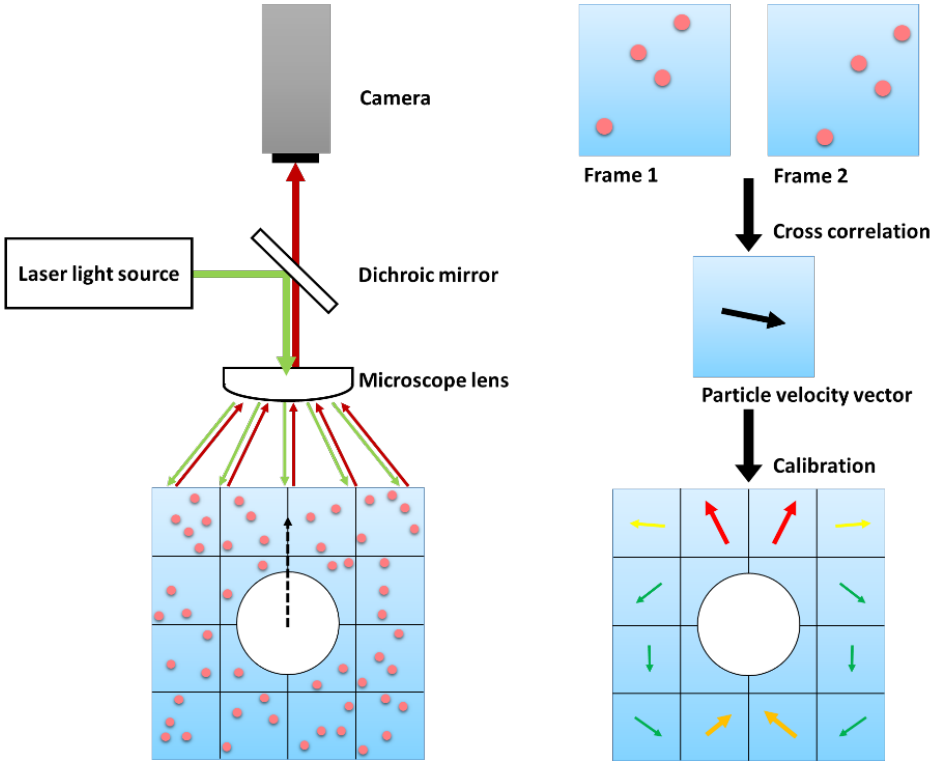

Figure S3. (Left) Schematic representation of the light path from the laser to the camera. **(Right)** Schematic step-by-step explanation of PIV

Imaging

The µPIV-system was calibrated using LaVision's 50 µm calibration plate, which includes mark spacing. When using 10x/0.30 objective, the scale factor is 1.59 pixel μm^{-1}. The total image size was 1376 x 1040 pixels or 863 µm x 652 µm.

Throughout the experiments, the particles had a diameter of 2-4 pixels. The number of particles in a 128px by 128px interrogation window was around 10. The time interval between a double frame was adjusted so that the displacement of the particles did not exceed 25% of the largest interrogation window. In the validation experiments at 0 mA cm^{-2}, a double frame time interval between 2 ms and 90 ms was used. In the other experiments, the time interval was varied between 0.5 ms and 10 ms. In every experiment a video of 100 to 200 double frames was taken (20 - 40 s).

Pre-processing of the double images

The images were pre-processed in the DaVis software in three steps (see **Figure S4**):

1. Masking – To ensure only particles in the fluid were tracked, a geometric mask was applied over the electrode.

2. Subtract time filter – To minimize background noise, the average intensity of each pixel position over all frames (100 to 200 double images) was subtracted from all images.

3. Subtract pixel intensity – Because of lens effects and particles in front and behind the focal plane, small clouds appear. To make sure only particles in focus were tracked, we subtracted between 10 to 25 counts from all pixels. This significantly improved the signal-to-noise ratio.

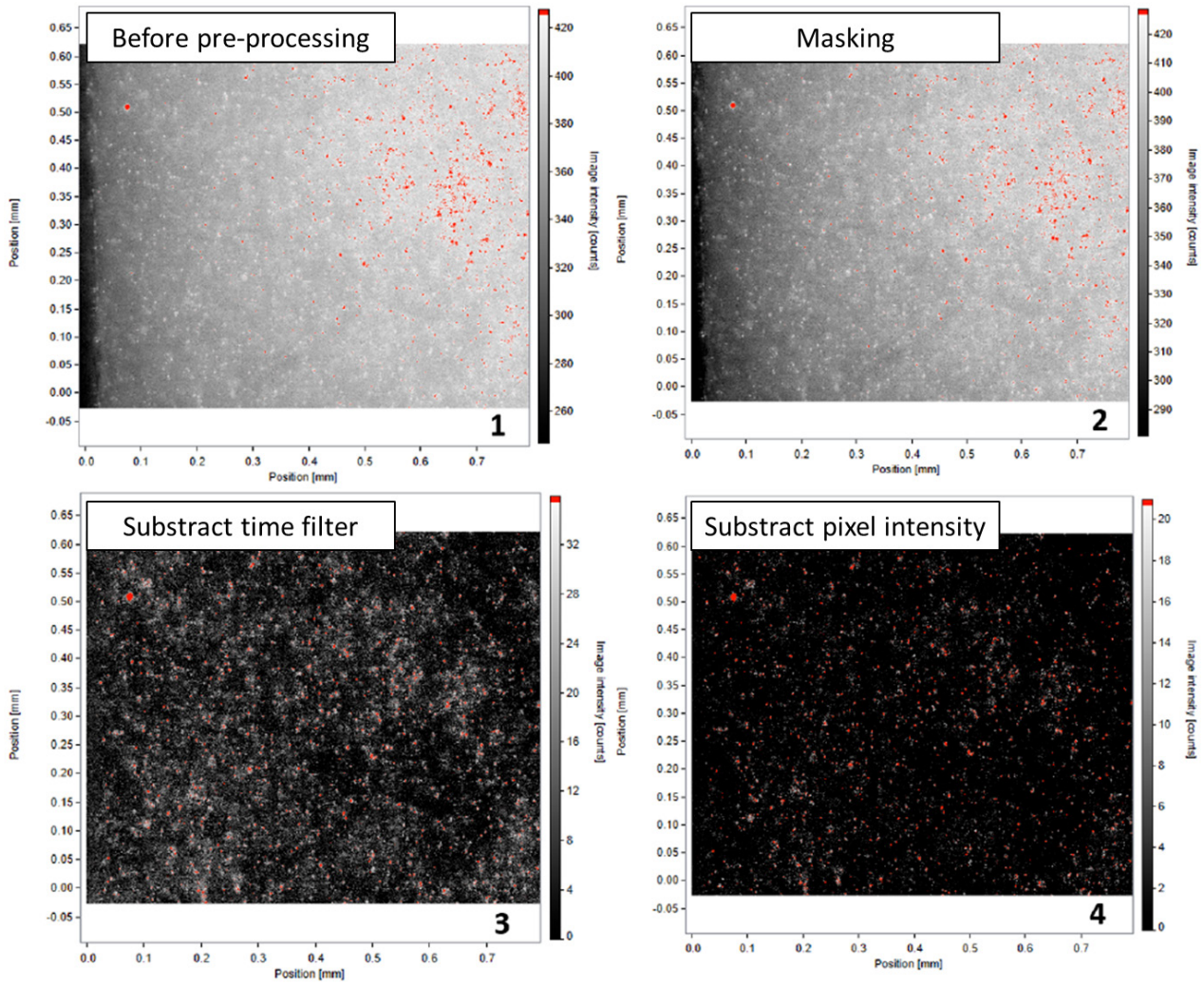

Figure S4. µPIV pre-processing steps

PIV cross-correlation

The velocity vector fields were calculated with cross-correlation in the DaVis software[1]. This was done in two steps: First a 512 x 512 interrogation window was used with 50% overlap, then an interrogation window of 128 x 128 was used with four passes with a 75% overlap. The data from the 512 x 512 interrogation window was used to find the best correlation near the predicted vector in the 128 x 128 interrogation windows. After cross-correlation the data was post processed with a 5x5 median filter.

SI-3. COMSOL model explanation

Here we describe the parameters, equations and boundary conditions used the in COMSOL model. 2D concentration fields were calculated from the velocity fields obtained in the µPIV measurements. Our system is modelled as a water electrolyser, similar to the FLIM experiments, generating OH^- at the electrode (**Figure S5**). We acknowledge that these equations strongly simplify a water electrolysis system, and serve only to understand the magnitude of mass transport from the obtained velocity fields from µPIV.

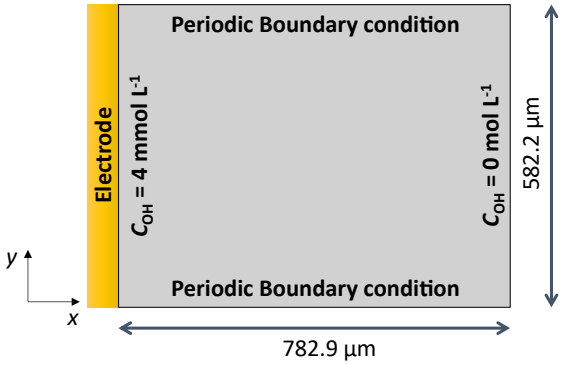

Figure S5. Graphical representation of the domain and boundary conditions of the COMSOL model

Model Geometry

The model has a rectangular geometry, which matches the visualized area in the PIV experiments, which was 582.2 µm by 782.9 µm. The model uses a triangular physics controlled "extra fine" mesh. All meshes were generated automatically by COMSOL. The "extremely fine" mesh did not yield significantly different results, hence we used the coarser mesh to reduce computation time. The mesh consisted of 4666 domain elements and 174 boundary elements,

Material

We model the transport of OH^- in water, diffusion coefficient (D_{OH}) 5.27 10^{-9} m^2 s^{-1} (Source: Aqion.de).

Governing equations & boundary conditions

The transport of OH^- is calculated with the "Transport of diluted species" module of COMSOL:

$$\frac{\partial N_{\mathrm{OH}}}{\partial y} + \frac{\partial N_{\mathrm{OH}}}{\partial x} + v_y \frac{\partial c_{\mathrm{OH}}}{\partial y} + v_x \frac{\partial c_{\mathrm{OH}}}{\partial x} = R_{\mathrm{OH}} \qquad \textbf{Eq S1}$$

Convective transport is calculated with the experimentally obtained velocity field. As initial value for the calculations, we used C_{OH} = 0. The left boundary is a constant concentration (C_{OH}(x=0) = 4 mmol L^{-1}) to mimic the experimentally measured concentration at electrode in the FLIM measurements in **Figure 3**. On the right side, a constant concentration boundary condition with the bulk concentration was used (C_{OH}(x=L) = 0). The top and bottom have a periodic boundary condition (**Figure S5**).

Importing the µPIV velocity field

The velocity fields were exported from the DaVis PIV-software as *x*-coordinate, *y*-coordinate, v_x and v_y. Before loading the data into COMSOL, the outliers of the velocity field are removed. The vectors with the highest and lowest 1% v_x values were removed, because we observed the µPIV experiments would sometimes result into few incorrectly large velocity vectors, especially near the electrode and

the boundaries of the image. After processing the data, the velocity vectors are imported to COMSOL. These velocity vectors were converted into a 2D velocity field with linear interpolation in the software.

Post-processing of the model results

A 2D concentration field was obtained after running the model. The boundary layer was extracted by plotting a contour line at 5% of 4mmol L^{-1}, which was exported as x- and y-coordinates. Since the y-coordinates were spaced irregularly, we calculated the effective boundary layer thickness (δ_{eff}) with a discretized version of **Eq 5** (see derivation in next section):

$$\delta_{\mathrm{eff}} = L\left(\sum_{i=1}^{N} \frac{L_i}{\delta_i}\right)^{-1} \qquad \textbf{Eq S2}$$

Here δ_{eff} is the effective boundary layer thickness, L is the total y-length of the boundary layer profile, L_i is the y-distance between two datapoints and δ_i is the boundary layer thickness at that datapoint.

Derivation of effective boundary layer thickness (δ_{eff})

To derive the equation for δ_{eff}, we assumed that inside the mass-transport boundary layer all mass transport is through diffusion. At a given height y along the electrode, the mass flux will be given by Fick's law:

$$N(y) = -D\left(\frac{dc}{dx}\right) \cong -D\frac{\left(c_{\mathrm{bulk}} - c(x=0)\right)}{\delta(y)} = D\frac{c(x=0)}{\delta(y)} \qquad \textbf{Eq S3}$$

Here, $N(y)$ is the flux at point y, D is the diffusion coefficient, c is the concentration, c_{bulk} is the bulk concentration outside the boundary layer (which is 0) and $\delta(y)$ is the boundary layer thickness at point y. If we want to calculate the average mass flux (N_{avg}) along an electrode with length L, we can integrate the **Eq S3**:

$$N_{\mathrm{avg}} = \frac{\int_0^L N(y)\mathrm{d}y}{L} = \frac{Dc(x=0)\int_0^L \frac{1}{\delta(y)}\mathrm{d}y}{L} \qquad \textbf{Eq S4}$$

If we discretize this integral, the equation becomes:

$$N_{\mathrm{avg}} = \frac{Dc(x=0)\sum_{\mathrm{i}=1}^{N} \frac{L_{\mathrm{i}}}{\delta_{\mathrm{i}}}}{L} \qquad \textbf{Eq S5}$$

Here δ_i is the boundary layer thickness for point i and L_i is the distance until the next datapoint. If we now rewrite N_{avg} like Fick's law, we get the following equation:

$$N_{\mathrm{avg}} = D\frac{c(x=0)}{\delta_{\mathrm{eff}}} \qquad \textbf{Eq S6}$$

By then combining **Eq S5** and **S6** we get:

$$\frac{1}{\delta_{\mathrm{eff}}} = \frac{\sum_{i=1}^{N} \frac{L_i}{\delta_i}}{L} \rightarrow \delta_{\mathrm{eff}} = L\left(\sum_{i=1}^{N} \frac{L_i}{\delta_i}\right)^{-1} \qquad \textbf{Eq S7}$$

SI-4. OH^- concentrations during FLIM experiments

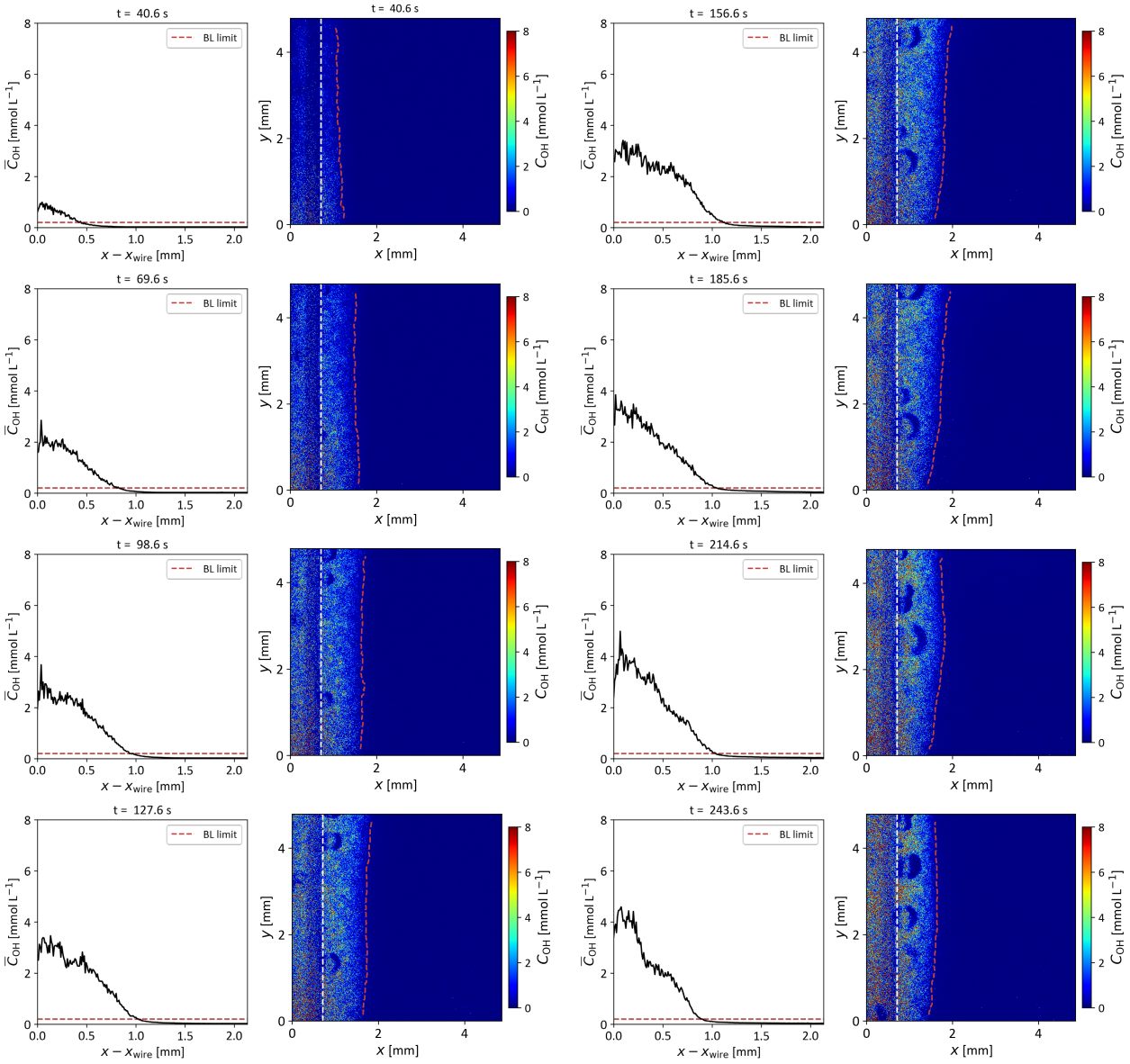

Figure S6. C_{OH} averaged over the length (y-averaged) of the electrode vs x, for various timestamps, and 2D C_{OH} plots at various timestamps during the FLIM experiment of Figure 3. The red dashed line in the C_{OH} vs x plot indicates the cut-off point of the boundary layer. In the 2D concentration plots, the white and red line are the electrode surface and boundary layer cut-off respectively.

SI-5. µPIV method validation

Here we validate our approach to use µPIV for mass transport research. We want to show that the fluctuations originating from the forced convection have minimal impact on the resulting concentration plots. This way we can confirm that our method only sees the effect of gas bubbles, and is not influenced significantly by the pumping of electrolyte. The flow needs to fulfil the following requirements:

- A relatively stable, unidirectional flow ($v_y >> v_x$, dv_y/dy = small). This will allow us to distinguish the effects from gas bubbles, from deviations in the velocity due to non-steady flow.
- The flowrate needs to be large enough to avoid heating up from the laser light source, which could result in natural convection.

Figure S7A and **S7B** show an image taken and the corresponding v_x and v_y velocity field, which shows that the flow is almost unidirectional, but still has small (<0.1 mm s^{-1}) fluctuations in the v_x. **Figure S7C** and **S7D** show the v_x and v_y over the width of the frame, averaged over the height of the frame and over 25 frames (5 s). The beginning of a parabolic flow profile can be seen, which increases linearly with flowrate, indicating that the flow is fully developed and laminar.

However at 1 mL min^{-1} we observed small effects of natural convection due to heating from the light source. We therefore chose to do all bubble induced mass transport experiments at flowrates of 2 mL min^{-1} or higher. The horizontal velocity v_x is around 0 mm s^{-1}, but the deviations increase at higher flowrates. We decided to not measure at flowrates above 5 mL min^{-1} to minimize effects of forced convection on the concentration plots. **Figure S7E** shows the calculated concentration field after implementing the time-dependent velocity profiles from **Figure S7B**. An almost linear profile can be observed, indicating that mass transport is mostly by diffusion, hence the small fluctuations in v_x do not significantly influence the calculated boundary layer thickness. **Figure S7F** shows that the boundary layer thickness over 25 frames (5 s) is not strongly influenced by flow fluctuations, and its influence is at least an order of magnitude smaller than the effect of gas bubbles.

Hence we confirm that we developed a system that can be used to investigate the effect of gas bubble dynamics on mass transport, without being affected by the small fluctuations in the flow due to forced convection or heating.

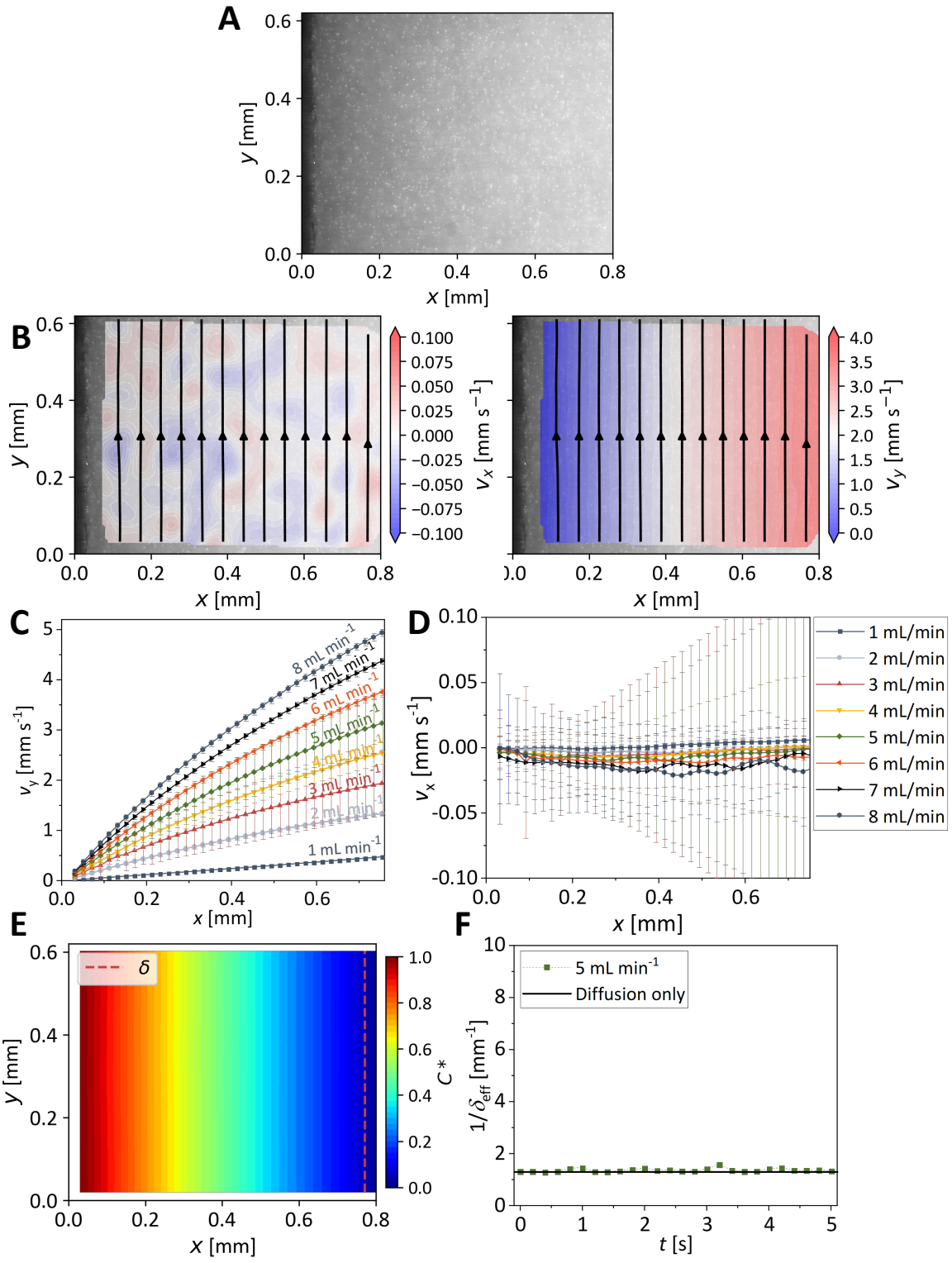

Figure S7. A. µPIV image of the electrode with a 5 mL min^{-1} flowrate and no applied current (0 mA cm^{-2}) at t = 4 s. **B.** Corresponding velocity fields (left: v_x, right: v_y). Streamlines indicate the flow direction, the color contour is the velocity component **C.** y-velocity and **D.** x-velocity over the width of the image at different flowrates, averaged over 25 frames (5 s), the error bars indicate the standard deviation. **E.** Resolved concentration profile after implementing the flowfield of B in the mass transport model, dashed red line indicates the boundary layer **F.** $1/\delta_{eff}$ when applying no current, compared to a system with only diffusion (all velocities in the model are set to 0).

SI-6. Effect of bubble diameter on fluid velocities

To find the relation between the velocity of the bubble (v_t), and the lateral velocity of the fluid(v_x) we perform order-1 scaling on the 2D-continuity equation:

$$\frac{\partial v_x}{\partial x} + \frac{\partial v_y}{\partial y} = 0 \qquad \textbf{Eq S8}$$

If we nondimensionalize this, the equation becomes:

$$\frac{[v_x]}{[x]}\frac{\partial v_x^*}{\partial x^*} + \frac{[v_y]}{[y]}\frac{\partial v_y^*}{\partial y^*} = 0 \qquad \textbf{Eq S9}$$

Here a * indicates the nondimensional variable, and the square brackets indicate the velocity length scale or the velocity magnitude. We then apply the O(1) scaling:

$$\frac{[v_x]}{[x]} \sim \frac{[v_y]}{[y]} \qquad \textbf{Eq S10}$$

In our measurements, we observed that velocity profiles are present about one d_{bubble} around the bubble, therefore [x] and [y] are both proportional to d_{bubble}. The y-velocity is proportional to the terminal velocity. Thus:

$$[v_y] = v_t \quad [x] = [y] = d_{bubble} \qquad \textbf{Eq S11}$$

And:

$$[v_x] \sim v_t \qquad \textbf{Eq S12}$$

We also developed a 3D continuum CFD model in COMSOL to simulate a gas bubble rising near a wall and to find the scale of the lateral velocity [v_x]. To simplify the model, we used a Lagrangian reference frame (i.e. the model follows the bubble, so the bubble appears stationary while the surrounding fluid and wall are moving downwards). The bubble was modelled as a solid sphere. The gap between the bubble and the wall and the bubble was set to $0.1d_{bubble}$ and the velocity of the wall and fluid are $-0.36v_t$. **Figure S8B** shows a typical velocity profile calculated with the model, the shape closely resembles the observed profiles in µPIV. **Figure S8C** shows that the model finds maximum lateral velocities of around $0.085v_t$.

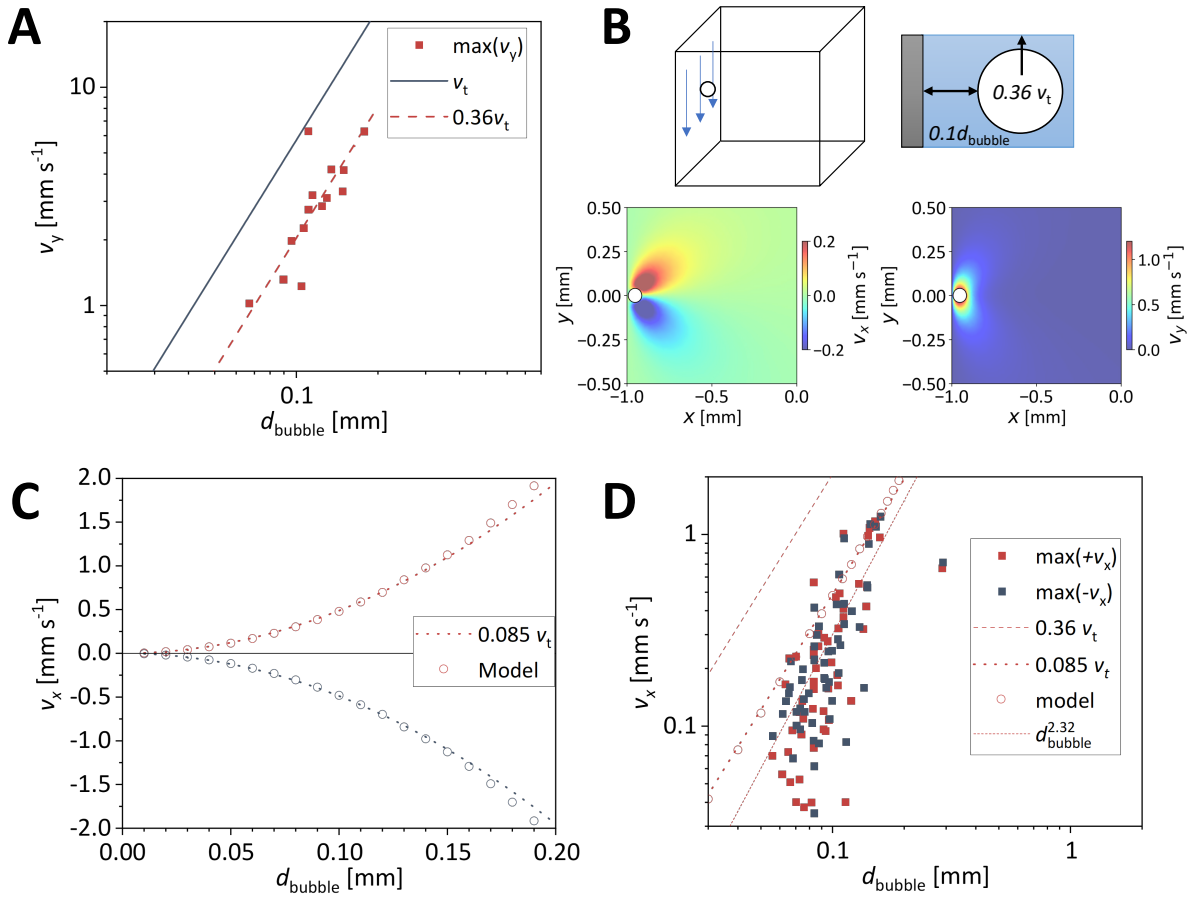

Figure S8A. log-log plot of **Figure 5B B**. Sketch of the Lagrangian model around a rising bubble, and examples of x and y-velocity profiles for a bubble with d_{bubble} of 80 µm **C.** Comparison of modelled velocities to 0.085v_t **D.** log-log plot of **Figure 5D**.

SI-7. FLIM Experiments at higher current densities

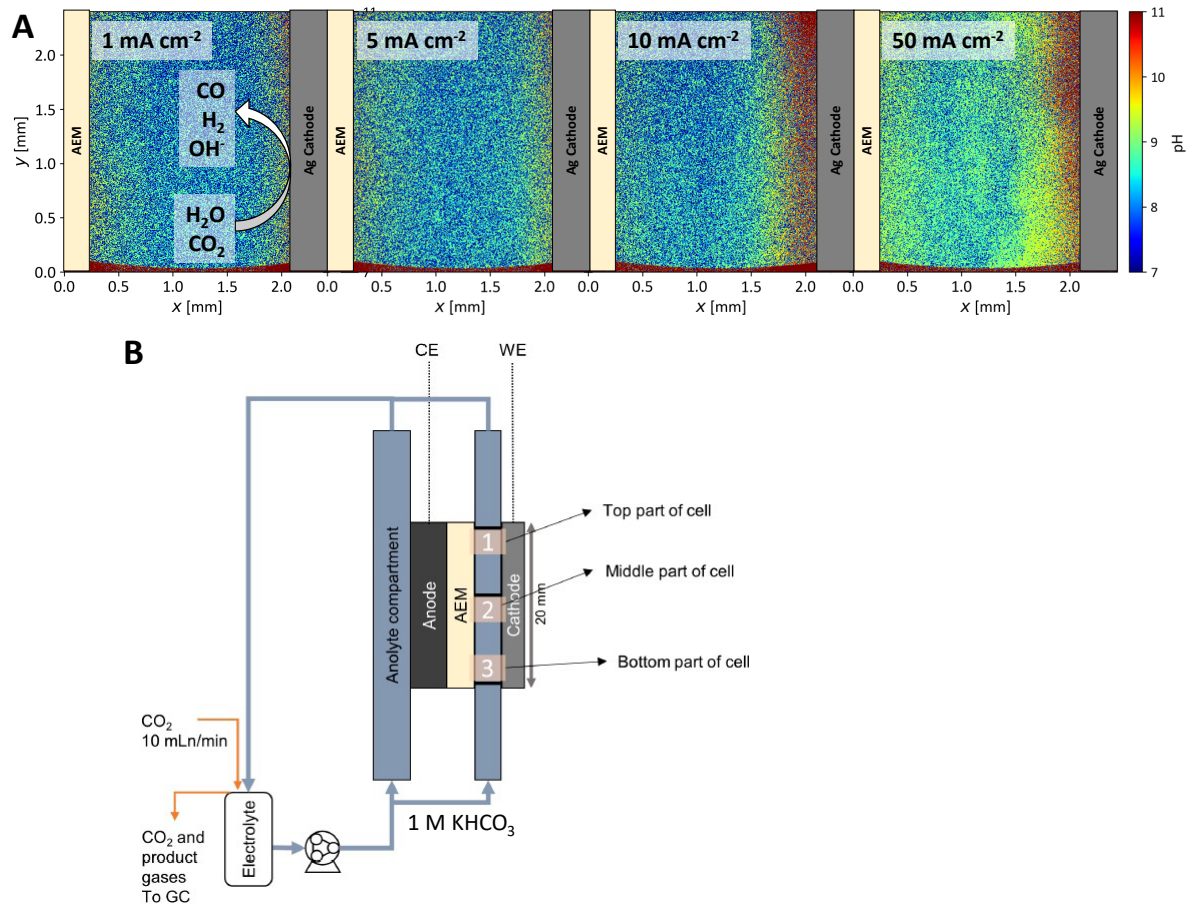

Figure S9A. 2D-pH resolved images with FLIM at increasing current densities. A CO_2 electrolyser catholyte compartment is visualized, with the setup from Baumgartner et al. with the gas compartment removed and the gas diffusion electrode replaced with a silver plate electrode[2] Note that these experiments used a different FLIM probe (**2c** from Bleeker et al.)[3]. The experiments are done on a Ag cathode in 1 M $KHCO_3$ saturated with CO_2 under a flowrate of 1.4 mL min^{-1} (Re = 8). Even during a of gas evolution at a current density 50 mA cm^{-2} a local pH boundary layer is still visible and can be resolved. **B.** Cross-sectional diagram of the setup used. All images in A are taken in the middle of the cell (2).

References

1. Raffel, M.; Willert, C. E.; Scarano, F.; Kähler, C. J.; Wereley, S. T.; Kompenhans, J., *Particle image velocimetry: a practical guide*. springer: 2018.
2. Baumgartner, L. M.; Kahn, A.; Hoogland, M.; Bleeker, J.; Jager, W. F.; Vermaas, D. A., Direct Imaging of Local pH Reveals Bubble-Induced Mixing in a CO2 Electrolyzer. *ACS Sustainable Chemistry & Engineering* **2023,** *11* (28), 10430-10440.
3. Bleeker, J.; Kahn, A. P.; Baumgartner, L. M.; Grozema, F. C.; Vermaas, D. A.; Jager, W. F., Quinolinium-Based Fluorescent Probes for Dynamic pH Monitoring in Aqueous Media at High pH Using Fluorescence Lifetime Imaging. *ACS Sensors* **2023,** *8* (5), 2050-2059.